Basin-scale ocean circulation from combined altimetric, tomographic and model data

Dimitris Menemenlis*, Tony Webb†, Carl Wunsch*, Uwe Send‡ & Chris Hill*

** Department of Earth, Atmospheric, and Planetary Sciences, Massachusetts Institute of Technology, Cambridge, Massachusetts 02139, USA*
† Civil Engineering, University College, UNSW, ADFA, Northcott Drive, Campbell, ACT, 2601, Australia
‡ Institut für Meereskunde, Regionale Ozeanographie, Duesternbrooker Weg 20, 24105 Kiel, Germany

The ocean stores and transports vast quantities of heat, fresh water, carbon and other materials, and its circulation plays an important role in determining both the Earth's climate and fundamental processes in the biosphere. Understanding the development of climate and important biological cycles therefore requires detailed knowledge of ocean circulation and its transport properties. This cannot be achieved solely through modelling, but must involve accurate observations of the spatio-temporal evolution of the global oceanic flow field. Estimates of oceanic flow are currently made on the basis of space-borne measurements of the sea surface, and monitoring of the ocean interior. Satellite altimetry and acoustic tomography are complementary for this purpose[1], as the former provides detailed horizontal coverage of the surface, and the latter the requisite vertical sampling of the interior. High-quality acoustic-tomographic[2] and altimetric[3] data are now available to test the combined power of these technologies for estimating oceanic flows. Here we demonstrate that, with the aid of state-of-the-art numerical models, it is possible to recover from these data a detailed spatio-temporal record of flow over basin-scale volumes of fluid. Our present results are restricted to the Mediterranean Sea, but the method described here provides a powerful tool for studying oceanic circulation worldwide.

The ocean fluctuates on a wide range of spatial and temporal scales[4]. The measured potential-energy spectrum of the circulation is mostly 'red', that is, the energy density increases with increasing spatial and temporal scales, but with a marked peak at the annual cycle. However, the kinetic-energy spectrum is dominated by mesoscale eddies with horizontal scales of 100 km or so, and periods of weeks to months. Therefore, studies of the large-scale movement of the sea need to resolve the mesoscale eddies and other narrow features of the circulation such as boundary-layer jets which are responsible for a large fraction of the heat and property transport. To resolve these features, the ocean would have to be instrumented roughly every 50 km horizontally and at some 20 levels vertically. The requirements for global coverage at this resolution are prohibitive.

Here we focus on the use of tomographic and altimetric observation systems which, in combination with more traditional ocean sampling methods, go far towards solving the global observation problem. Satellite altimetry measures the sea surface elevation relative to the geoid, that is, relative to the particular gravitational equipotential to which the sea surface would conform if it were at rest with no forces acting on it (other than gravity). Changes in

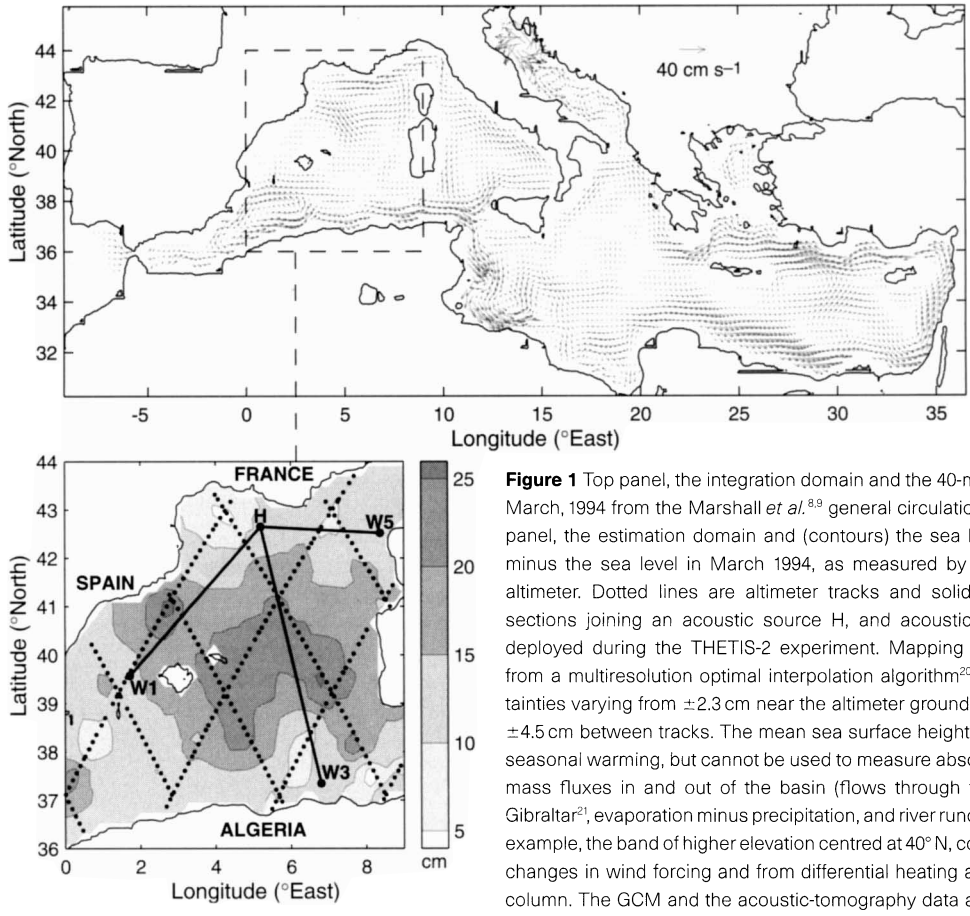

Figure 1 Top panel, the integration domain and the 40-m horizontal velocity on 1 March, 1994 from the Marshall *et al.*[8,9] general circulation model (GCM). Bottom panel, the estimation domain and (contours) the sea level in September 1994 minus the sea level in March 1994, as measured by the TOPEX/POSEIDON altimeter. Dotted lines are altimeter tracks and solid lines are tomographic sections joining an acoustic source H, and acoustic receivers W1, W3, W5 deployed during the THETIS-2 experiment. Mapping of the altimeter data is from a multiresolution optimal interpolation algorithm[20]. Estimates have uncertainties varying from ±2.3 cm near the altimeter ground tracks to a maximum of ±4.5 cm between tracks. The mean sea surface height increase is indicative of seasonal warming, but cannot be used to measure absolute heating because of mass fluxes in and out of the basin (flows through the Straits of Sicily and Gibraltar[21], evaporation minus precipitation, and river runoff). Relative changes, for example, the band of higher elevation centred at 40° N, contain contributions from changes in wind forcing and from differential heating and cooling of the water column. The GCM and the acoustic-tomography data are used to separate the respective contributions to sea-level anomaly of wind and heat content.

elevation result from local exchange of mass and heat with the atmosphere through the sea surface, and from lateral water movements. In general terms, surface elevation and its slope provide a dynamical surface boundary condition on the general circulation.

The second observational system, ocean acoustic tomography, integrates the oceanic state along many paths through a volume of fluid by transmitting sound pulses from sources to receivers. Perturbations in travel time of acoustic pulses are dominated by temperature perturbations, and to a lesser degree by perturbations in density and velocity[5]. Both altimetric and tomographic measurements have been compared in detail (where possible) to more conventional oceanographic measurements and have been shown to be fully consistent with them[2,6].

We used altimetric data[7] from the tracks shown in Fig. 1 for the period 3 October, 1992 to 25 November, 1994. The measured sea-surface height change during a six-month period, March to September 1994, concurrent with the tomographic measurements is also shown in Fig. 1. Because of the residual geoid errors and because mass is not conserved in the western Mediterranean basin, the altimeter data do not directly reflect the mean circulation or the basin-averaged changes in heat content[6].

We also use the analysis of THETIS-2 acoustic tomography data shown in Fig. 2 and consisting of depth-averaged (0–2,000 m) and path-averaged potential temperature along the three sections marked on Fig. 1. The tomographic data, over the instrumented period from February to October 1994, show, in addition to the expected seasonal warming through summer, a marked difference between the mid-basin section (H-W3) and the northern sections—a difference that mirrors the relative amplitude variations from the altimetry.

To recover an ocean state which is dynamically consistent with the observations, we use the general circulation model (GCM) of Marshall *et al.*[8,9], which is here integrated for the entire Mediterranean basin with realistic topography, 0.25° horizontal grid spacing, and 20 vertical levels (Fig. 1). Twice-daily surface wind-stress boundary conditions are from the European Center for Medium Range Weather Forecasts (ECMWF), and heat and freshwater fluxes are provided by a relaxation term at the surface to seasonal climatologies[10] of temperature and salinity in order to mimic seasonal heat and freshwater fluxes. An Atlantic box is added to simulate the Gibraltar throughflow. The GCM includes a simple convective overturning scheme permitting buoyancy-driven deep-water formation to take place, but lacks a wind-driven mixed layer. In this configuration the GCM reproduces a wind-driven circulation consistent on the large scales with that obtained by previous modelling studies[11,12], but fails to capture the detailed thermo-

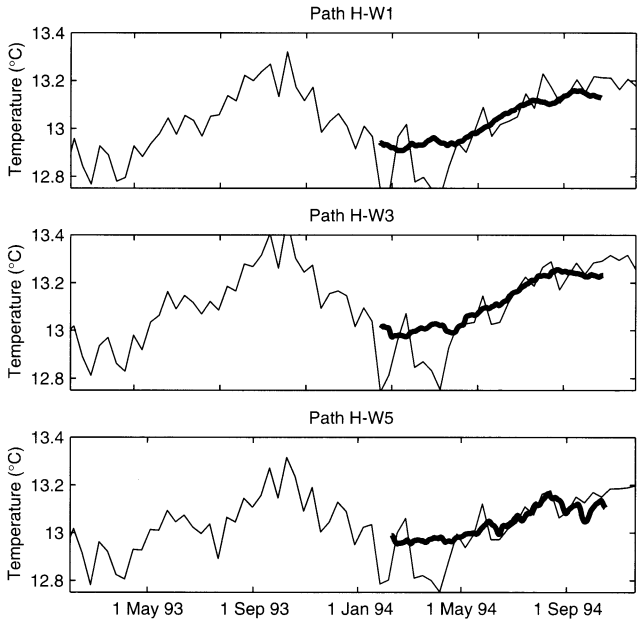

Figure 2 Depth-averaged (0–2,000 m) and path-averaged potential temperature measured using ocean acoustic tomography (thick lines) and estimated from the altimeter data (thin lines) along the three sections marked on Fig. 1. Tomographic heat content estimates are from inversions using a single deep-diving acoustic ray. The estimated uncertainty is ±0.013 °C. Section H-W3 was sampled on a regular basis with expendable bathythermographs during the duration of the experiment and the agreement with the inversions is to within measurement uncertainty. The data show a strong seasonal heating which is mainly confined to the top 50 m and is consistent with ECMWF heat flux analyses over the western Mediterranean[2]. Altimeter heat content estimates are made under the assumption that the sea-level anomaly signal results from uniform heating or cooling of the top 50 m. Differences between the tomographic and the altimetric heat content estimates result from physical processes other than heating or cooling of the surface layer, for example, the response of the sea-level anomaly to changes in atmospheric pressure, wind stress, and freshwater fluxes. A key contribution of the tomographic data is the ability to estimate the heat content part of the altimetric sea-level anomaly signal.

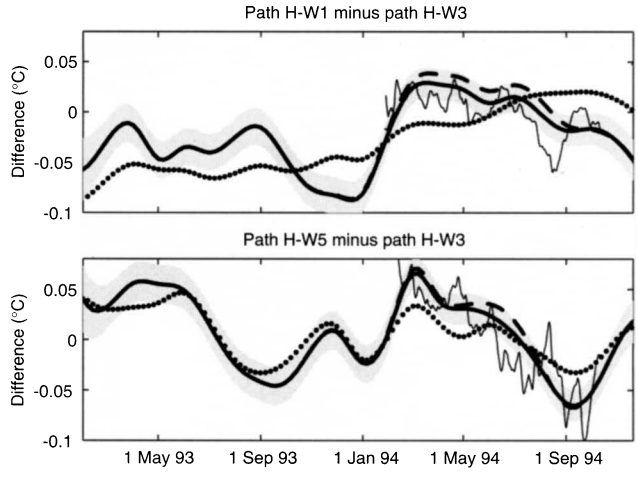

Figure 3 Difference between depth-averaged (0–2,000 m) and path-averaged potential temperature along the tomographic sections. The dotted line is the GCM estimate; the dashed line indicates the GCM/altimeter combination; the thick solid line represents the GCM/altimeter/tomography combination with the shaded area indicating the standard error of this last estimate; the thin solid line is the tomographic data; and circles represent altimeter data converted to depth-integrated temperature as in Fig. 2. GCM and data biases have been removed as discussed in the text. The GCM predictions differ significantly from the tomographic data because of the lack of realistic buoyancy forcing at the surface. However, the GCM/altimeter combination successfully recovers the time-evolving spatial anomaly of heat content, as seen through the calibration against tomographic data. The addition of the tomographic data does not change the estimates significantly, but the uncertainty is reduced by 17%, from ±0.018 °C when there are no tomographic data to ±0.015 °C during the period when tomographic data are available. Remaining differences between the estimates and the tomographic data are believed real–representing the still-inadequate resolution of the GCM and of the estimation method.

dynamic surface forcing and seasonal heating and cooling of the surface layer. The estimation scheme, described below, compensates in part for these and other GCM deficiencies, as well as the shortcomings of the data.

The problem of combining data and models is analogous to, but distinct in practice, from that used to depict the atmosphere for purposes of numerical weather forecasting. The spatial scales of oceanic variability are much smaller than in the atmosphere, while the temporal scales are much longer. Furthermore, we are not (yet) interested primarily in forecasting, but in understanding, so that the estimation ('assimilation') methods have the goal of the most accurate state estimate, rather than the most accurate forecast. We thus exploit the ability to use formally future data, that is, estimates at any given moment are influenced by all the observations, past, present, and future to the estimation time period.

A least-squares fit of the available data is made to a reduced-state, linear model. The reduced state describes large-scale, low-frequency temperature (density) differences between the GCM and the observations, and is represented by four vertical modes, 1°-sampling in the horizontal, and 1-month time steps. This state reduction is required to make the problem tractable with the available computational resources. The reduced-state linear model is determined by systematically perturbing the GCM and using the resulting anomalies to deduce a state transition matrix for the physical processes governing the perturbations[13]. It is assumed, and tested *a posteriori*, that the GCM is sufficiently close to the observations for the linearization to be adequate. The least-squares problem is solved using a sequential algorithm—the Kalman filter followed by the Rauch–Tung–Striebel smoother[14]—to obtain estimates of the reduced state and the associated uncertainty covariance matrix. Discrepancies between the GCM and observations of freshwater fluxes, external modes, and other physical processes not resolved by the reduced state are part of the error budget in this analysis.

Two difficulties are encountered. First, it is necessary to specify second-order error statistics for the reduced state model, the control terms, and the measurement error. These statistics are imposed here in the form of diagonal covariance matrices estimated from the observations themselves. With more data, more realistic second-order statistics could be obtained using adaptive filter theory[15].

The second difficulty is the existence of large GCM and data biases (primarily large-scale temperature offsets and missing wind-driven mixed-layer processes in the GCM, and geoid and atmospheric load errors in the altimetry) which need to be removed in the present approach. This is accommodated by decomposing the reduced state temperature, $T(\mathbf{r}, z, t)$, into a time-mean, $T_m(\mathbf{r}, z)$, a time-evolving, $T_e(z, t)$, and a residual term, $T'(\mathbf{r}, z, t)$:

$$T(\mathbf{r}, z, t) = T_m(\mathbf{r}, z) + T_e(z, t) + T'(\mathbf{r}, z, t) \quad (1)$$

where $\mathbf{r}$ is a horizontal position vector, z is depth, and t is time. $T_m(\mathbf{r}, t)$ is a correction for the large-scale offset of the GCM, and $T_e(z, t)$ is a correction for the inadequate GCM representation of seasonal warming in the mixed layer. The analysis is performed so that $T_m(\mathbf{r}, z)$ and $T_e(z, t)$ are rendered invisible in the data, thus eliminating the GCM/data biases, with the focus here being on estimating $T'(\mathbf{r}, z, t)$. The representation in equation (1) is neither unique nor rigorous, but it is adequate for determining the major modes of oceanic 'time variability'.

To test the accuracy of the constrained solution, the GCM/data combination is effected in two stages. In the first stage, the tomography data are withheld, and the GCM/altimetric combination is used to predict the spatial anomalies of the tomographic data (Fig. 3). The tomography shows the gradual heating of tomographic section H-W3 relative to the other two from February to October 1994. The GCM alone (without the altimetric data) fails to predict this relative warming trend, but the GCM/altimetric combination is consistent with the tomographic integrals.

In the second stage, both the altimetric and the tomographic data are used (Fig. 3). The addition of the tomographic data does not

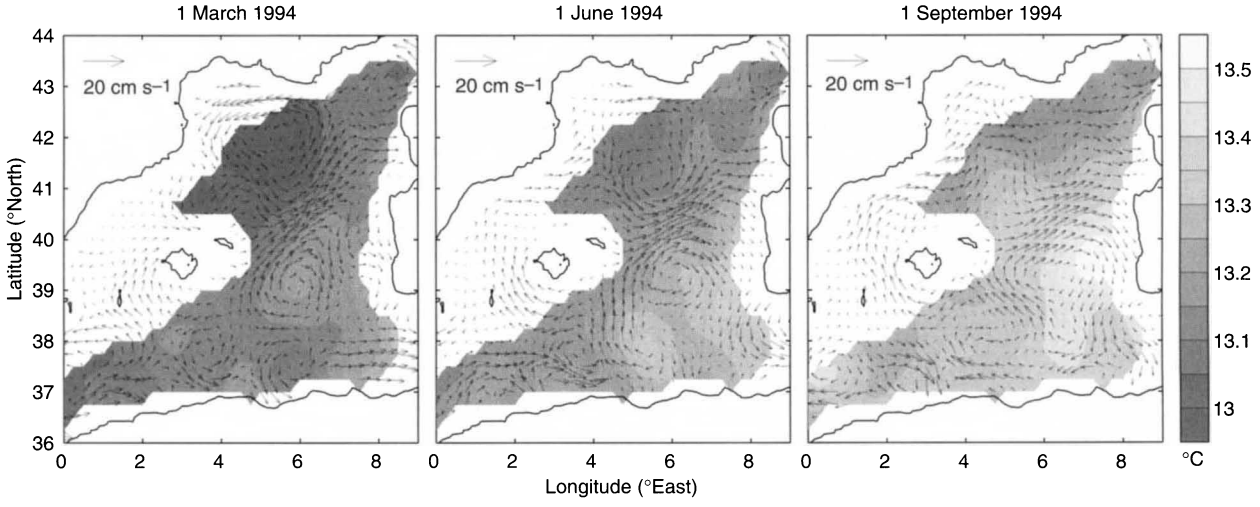

Figure 4 Estimates of western Mediterranean circulation, on 1 March, 1 June and 1 September, 1994, obtained by combining observations and the GCM. The grey-scale shading indicates depth-averaged (0–2,000 m) potential temperature and the arrows indicate horizontal velocity at 40 m depth. To summarize the key contributions of data and GCM, hydrographic data are used to estimate the time-mean temperature, the tomographic integrals provide the time-evolving temperature, the altimetry provides horizontal resolution, and the GCM determines the effect of observed winds and provides a reduced-state linear model which is used to interpolate the data to regions without measurements. The resulting estimates reproduce known features of the western Mediterranean circulation. For example the coldest waters are detected in the Gulf of Lions, a region where deep convection is known to occur every year[22], and are associated with the existence of a strong cyclonic gyre on 1 March, which gradually subsides later in the year. The warmest temperatures are observed in the southeastern part of the domain where the Levantine Intermediate Water enters the Algero-Provençal basin[23]. The present estimates are preliminary and their detailed analysis and interpretation is beyond the scope of this Letter, nevertheless these estimates illustrate the combined power of ocean acoustic tomography, satellite altimetry and GCMs for oceanographic studies.

significantly change the estimates of the residual temperature $T'(\mathbf{r}, z, t)$, but it does reduce the uncertainty.

The remaining contributions to the Mediterranean circulation, $T_m(\mathbf{r}, z)$ and $T_e(z, t)$ in equation (1), are estimated without the assistance of the GCM. The tomographic data provides estimates of the time-evolving component $T_e(z, t)$, and a climatological analysis of hydrographic data[10] provides an estimate of the time-mean component $T_m(\mathbf{r}, z)$. Last, the circulation is recovered using $T(\mathbf{r}, z, t)$ and the climatological salinity to compute density perturbations, and to obtain geostrophic corrections for the GCM circulation (the depth-integrated GCM transport is unchanged). Thus, to within the error bars and for the scales and processes resolved by the reduced state and by the climatologies, we obtain a complete description of the time-evolving three-dimensional Mediterranean circulation (Fig. 4).

Notwithstanding shortcomings in the existing models and data, the present results indicate that useful estimates of basin-scale oceanic circulation are already possible. Model and data deficiencies will diminish in time, but will always exists. The major issue is that the statement about model and data errors must be quantitative. Our results can be refined in several ways. In particular, a higher-resolution GCM with more realistic surface forcing, mixed-layer physical processes, and eddy parametrization will reduce GCM/data discrepancies. The estimates will also be improved when a more complete analysis of the THETIS-2 tomographic data becomes available, that is, more sections and higher vertical resolution. The estimation procedure itself can be augmented to account for smaller scales and more complete physical processes[16,17], to use better *a priori* statistics, or to obtain joint estimates of the three terms in equation (1).

The advent of high-accuracy altimeter missions and the improvement in GCM capability[18] have brought oceanographers nearer to the goal of a true global observing system. What is still missing is the continuous coverage within the oceanic water column necessary to complement the global horizontal observations from space. The Acoustic Thermometry of Ocean Climate[19] (ATOC) observations, now underway in the Pacific Ocean, in conjunction with the altimetry and developing models, will over the next several years produce a full oceanic-basin version of just such a system. The type of estimates we have made for the western Mediterranean Sea are now feasible for the entire North Pacific Ocean. □

Received 18 June; accepted 26 November 1996.

1. Munk, W. & Wunsch, C. *Phil. Trans. R. Soc. Lond. A* **307,** 439–464 (1982).
2. Send, U. *et al. Nature* **385,** 615–617 (1997).
3. Fu, L.-L. *et al. J. Geophys. Res.* **99,** 24369–24381 (1994).
4. Wunsch, C. & Stammer, D. *J. Geophys. Res.* **100,** 24895–24910 (1995).
5. Munk, W., Worcester, P. & Wunsch, C. *Ocean Acoustic Tomography* (Cambridge Univ. Press, New York, 1995).
6. Larnicol, G., Le Traon, P.-Y., Ayoub, N. & De Mey, P. *J. Geophys. Res.* **100,** 25163–25177 (1995).
7. Stammer, D. & Wunsch, C. *J. Geophys. Res.* **99,** 24584–24604 (1994).
8. Marshall, J., Hill, C., Perelman, L. & Adcroft, A. *J. Geophys. Res.* (in the press).
9. Marshall, J., Adcroft, A., Hill, C., Perelman, L. & Heisey, C. *J. Geophys. Res.* (in the press).
10. Brasseur, P., Beckers, J. M., Brankart, J. M. & Schoenauen *Deep-Sea Res. I* **43,** 159–192 (1996).
11. Zavatarelli, M. & Mellor, G. L. *J. Phys. Oceanogr.* **25,** 1384–1414 (1995).
12. Roussenov, V., Stanev, E., Artale, V. & Pinardi, N. *J. Geophys. Res.* **100,** 13515–13538 (1995).
13. Menemenlis, D. & Wunsch, C. *J. Atmos. Oceanic Technol.* (in the press).
14. Rauch, H. E., Tung, F. & Striebel, C. T. *Am. Inst. Aeronaut. Astronaut. J.* **3,** 1445–1450 (1965).
15. Blanchet, I., Frankignoul, C. & Cane, M. A. *Mon. Weath. Rev.* **125,** 40–58 (1997).
16. Marotzke, J. & Wunsch, C. *J. Geophys. Res.* **98,** 20149–20167 (1993).
17. Schiller, A. *J. Mar. Res.* **53,** 453–497 (1995).
18. Stammer, D., Tokmakian, R., Semtner, A. & Wunsch, C. *J. Geophys. Res.* **101,** 25779–25811 (1996).
19. Forbes, A. *Sea Technol.* **35,** 65–67 (1994).
20. Fieguth, P. W., Menemenlis, D., Ho, T., Willsky, A. & Wunsch, C. *J. Atmos. Oceanic Technol.* (submitted).
21. Bryden, H. L., Candela, J. & Kinder, T. H. *Prog. Oceanogr.* **33,** 201–248 (1994).
22. Send, U., Schott, F., Gaillard, F. & Desaubies, Y. *J. Geophys. Res.* **100,** 6927–6941 (1995).
23. Tziperman, E. & Malanotte-Rizzoli, P. *J. Marin. Res.* **49,** 411–434 (1991).

Acknowledgements. We thank our colleagues D. Stammer, C. King and P. Fieguth for help with the analysis of the TOPEX/POSEIDON altimeter data, and J. Marshall, C. Heisey and A. Adcroft for help with the GCM. This work was supported by the Strategic Environmental Research and Development Program and the Advanced Research Projects agency (ARPA) as part of the ATOC project; by NASA; and by grants of High Performance Computer time from Project SCOUT at the M.I.T. Laboratory for Computer Science, and from the Arctic Region Supercomputing Center.

Correspondence and requests for materials should be addressed to D.M. (e-mail: dimitri@gulf.mit.edu).

Rheology of the continental lithosphere inferred from sedimentary basins

Robert Newman & Nicky White

Department of Earth Sciences, Bullard Laboratories, University of Cambridge, Madingley Rise, Madingley Road, Cambridge CB3 0EZ, UK

The steady-state flow properties of the continental lithosphere play an important role in a wide range of geological processes[1]. A complete dynamic description of lithospheric deformation requires information about the magnitude of driving forces and the rheology of the crust and lithospheric mantle, about which there is little agreement[2–6]. Here we constrain these properties by analysing variations in strain rate during the extension of continental lithosphere. We determine the temporal variation of strain rate from the subsidence curves of a global sample of Phanerozoic sedimentary basins. The peak strain rate and final strain estimated from these strain-rate histories suggest that the cessation of extension is governed by cooling and concomitant strengthening of the underlying lithospheric mantle. Dynamic modelling of these data indicates that the rheology of the lithosphere is controlled by power-law creep with a stress exponent of three and an activation energy of ~500 kJ mol^{-1}. This rheology is consistent with that inferred from laboratory experiments on dry olivine[7] extrapolated to lithospheric conditions.

Kinematic models of lithospheric extension account satisfactorily for the structure and evolution of many sedimentary basins. But there is little agreement about the main aspects of the dynamical problem, namely the origin and magnitude of forces that drive extension and the rheology of the crust and lithospheric mantle[2–6]. We also do not know what limits the value of the stretching factor, β, defined as the ratio between initial and final crustal thickness. One possibility is that variation in strain rate is controlled by changes in the driving force. Alternatively, lithospheric mantle may cool and strengthen as the Moho rises, thereby reducing the strain rate produced by a given force[2]. If such cooling controls basin evolution, then we expect a characteristic change of strain rate with time[5]. Temporal strain-rate variation can therefore be used to test dynamic models[5].

The strength of the lithosphere (that is, the stress required to deform it at a given strain rate) is usually estimated from laboratory experiments in which quartz and olivine are deformed under high pressure at strain rates of 10^{-7}–10^{-4} s^{-1} and at temperatures of ⩾1,300 °C (ref. 7). Results show that the rheological properties of quartz and olivine can be described by empirical constitutive

Table 1 Principal parameters used in numerical experiments

a	Lithospheric thickness	125 km
t_c	Crustal thickness	33 km
A	Pre-exponential constant	1×10^5 MPa^{-3} s^{-1}
n	Stress exponent	3
Q	Activation energy	300–1,000 kJ mol^{-1}
R	Universal gas constant	8.314 J mol^{-1} K^{-1}
T_M	Initial Moho temperature	580 °C
T_L	Asthenosphere temperature	1,330 °C
k_c	Thermal conductivity of crust	2.5 W m^{-1} °C^{-1}
k_m	Thermal conductivity of mantle	3.0 W m^{-1} °C^{-1}
H	Crustal heat production	1.5 μW m^{-3}
T	Absolute temperature	K
β	Uniform stretching factor	
τ	Deviatoric stress	Pa
$\dot{\epsilon}$	Strain rate	s^{-1}